Coastal Engineering 183 (2023) 104330

Contents lists available at ScienceDirect

Coastal Engineering

journal homepage: www.elsevier.com/locate/coastaleng

Changes in seasonal compound floods in Vietnam revealed by a time-varying dependence structure of extreme rainfall and high surge

Han Wang [a,1], Yunqing Xuan [a,*], Thi Van Thu Tran [b], Anaïs Couasnon [c], Paolo Scussolini [c], Linh Nhat Luu [d,f], Hong Quan Nguyen [b,e], Dominic E. Reeve [a]

[a] Faculty of Science and Engineering, Swansea University Bay Campus, Swansea, SA1 8EN, UK
[b] Center of Water Management and Climate Change (WACC), Institute for Environment and Resources, Vietnam National University-Ho Chi Minh City (VNU-HCM), Ho Chi Minh City, 70000, Vietnam
[c] Institute for Environmental Studies (IVM), Vrije Universiteit Amsterdam, Amsterdam, the Netherlands
[d] Royal Netherlands Meteorological Institute, De Bilt, the Netherlands
[e] Institute for Circular Economy Development (ICED), Vietnam National University-Ho Chi Minh City (VNU-HCM), Ho Chi Minh City, 70000, Vietnam
[f] Vietnam Institute of Meteorology Hydrology and Climate Change, Hanoi, Vietnam

ARTICLE INFO

Keywords:
Coastal compound flood
Climate change
Quantification framework
Rainfall extremes
Storm surge

ABSTRACT

Compound floods due to intense rainfall and storm surges in coastal areas have shown an increasing trend in some parts of the world, and many studies suggested a strong link with climate change. Yet, such link has not been fully explored and quantitively assessed. In this paper, we demonstrate the development and application of a nonstationary framework to determining different compound scenarios, where individual drivers and their interactions have altered under climate change. The framework has been applied to one of the most flood-prone areas: the Ho Chi Minh City of Vietnam, to help analyze the present and future compound flood risks in both the dry and wet seasons driven by the joint effect from heavy inland rainfall and high skew surge. Over the period of 1980–2017, the two drivers are found to be significantly correlated in March and April, corresponding to the transition from dry-to-wet seasons. We also find that the commonly-used traditional multivariate statistical models underestimate the flood magnitudes for both the current (represented by 2020) and future (represented by 2050) scenarios, when compared with the results produced by the nonstationary methods. In addition, the results reveal that the dry season is expected to receive more floods triggered by the increased intensity and frequency of rainfall extremes, with the magnitude reaching a similar level to that of the wet season. This is in line with the climate projections under RCP4.5 and 8.5 scenarios although the duration of dry spells is expected to increase and the total annual rainfall to decrease in Vietnam. The simulated flood inundations indicate remarkable increases in flood magnitude and extension, especially at the locations identified as low risk by the stationary models.

1. Introduction

Coastal flooding is widely regarded as one of the most dangerous natural hazards in low-lying regions and often arises from various sources such as intense rainfall, storm surge, high sea level, and large river discharge either individually or in combination (Edmonds et al., 2020; Tiggeloven et al., 2020). Specifically, the concurrence or close succession of these different source mechanisms can lead to compound flooding, resulting in greater damage than from separate events caused by the individual mechanism (Hendry et al., 2019; Thomas Wahl et al., 2015). This is further exemplified by the occurrence of several recent events where floods were associated with hydrologic drivers (e.g., rainfall, river discharge) combined with oceanographic drivers (e.g., tides, surges, waves). Examples include the coastal compound floods on the North Carolina Coast of the USA (Gori et al., 2020); in the Shoalhaven estuary, Australia in June 2016 (Kumbier et al., 2018); the Noorderzijlvest, the Netherlands in 2015 (van den Hurk et al., 2015); and in Ravenna, Italy in 2015 (Bevacqua et al., 2020).

One of the most widely-used approaches to estimating the features of such high-impact coastal compound events usually rely on multivariate

* Corresponding author.
E-mail address: y.xuan@swansea.ac.uk (Y. Xuan).
[1] Present address: China Institute of Water Resources and Hydropower Research, Beijing 100038, China.

https://doi.org/10.1016/j.coastaleng.2023.104330
Received 24 January 2023; Received in revised form 20 April 2023; Accepted 23 April 2023
Available online 8 May 2023

analysis that calculates the maximum system response associated with a given exceedance probability by considering the interdependence, interaction and associations among different drivers or factors. Since climate system in coastal regions is extremely complicated and usually triggered by more-than-one source and their uncertain correlations (Ewans and Jonathan, 2014), many studies focus on developing models or frameworks to cope with multivariate statistical analysis by using various copulas (Sklar, 1959) in coastal areas (Jalili Pirani and Najafi, 2022; Jiang et al., 2021; Lucey and Gallien, 2022; Wahl et al., 2012). For example, Corbella and Stretch (2013) provided a multivariate statistical model by employing Archimedean copulas to quantify the dependencies between storm parameters i.e., wave height, wave period, storm duration, water level and storm inter-arrival time and applied to the east coast of South Africa. Masina et al. (2015) presented a copula-based approach to model the joint distribution between sea levels and wave heights from six-year records at one site of the Ravenna coast of Italy, where a one-parameter extreme value copula was selected to the best fit for constructing the dependence structure of extreme events. Tanim and Goharian (2021) developed an integrated modelling and multivariate analysis framework to analyze urban coastal floods driven by runoff and storm surge in Chittagong City of Bangladesh, which involves a hydrologic model and a coastal hydrodynamic model with the use of Gaussian copula. As the dependency between oceanographic and meteorological parameters is difficult to recognise (Ewans and Jonathan, 2014), some efforts have been made in exploring the realistic dependency in coastal studies, such as applying nonlinear dependency among sea states parameters by using asymmetric copulas (Zhang et al., 2018), using entropy copula to avoid the procedures of copula selection (Li et al., 2018), or getting rid of the statistical methods but directly coupling the several hydrological or hydrodynamic models (Ikeuchi et al., 2017; Shi et al., 2022; Zhang et al., 2020), which requires large computational time and capacity.

However, global warming and anthropogenic climate change have led to significant changes in regional climate of coastal areas which bring changes to not only the single flood-driven factors separately, but also their interactions (Utsumi and Kim, 2022; Zscheischler et al., 2018). Notably, the multivariate probability analysis applied in most of the literature mentioned above has been performed under the assumption of constant parameters; their assumption of stationarity potentially leading to less accuracy in capturing features of compound events. In recent years, many attempts have been made for endeavouring to capture climate change to compound floods in low-laying coastal regions. Some publications concentrate on directly involving climate models or projections of flood-drivers and implicitly considering their dependency (Bermúdez et al., 2021; Pasquier et al., 2019), while others focus on improving the multivariate statistical analysis by incorporating nonstationarity, and many have applied in hydrology-related studies like drought and inland floods (Feng et al., 2020; Kwon and Lall, 2016; Sarhadi et al., 2018). In coastal studies, for instance, Davies et al. (2017) developed a probabilistic framework to model the nonstationarity of univariate storm feature such as wave direction, height, duration, period which are tested to relate to El Niño-Southern Oscillation (ENSO) and seasonality, then make the nonstationary univariate distribution conditional on seasonal and climate covariates and finally employed a vine copula to generate the joint probability. Ghanbari et al. (2021) also incorporated nonstationarity in the marginal distribution of drivers and estimated the changes in compound coastal-riverine flooding hazard along the US coasts.

Compared with incorporating climate change in physical-based modelling, the statistical method is more time-saving and cost-efficient, however, it needs to be recognised that the dependency among flood-drivers can be also changing due to climate besides the nonstationary change of drivers themselves. And the quantification of combined change of both drivers and their interaction in the view of nonstationarity especially at the level of extreme, has not yet been fully studied. Motivated by this, we developed a feasible nonstationary framework in modelling complex compound extreme events where the possible combinations of stationary and nonstationary flood-drivers and their interactions are concerned. The framework was then applied to a case study of Ho Chi Minh City (HCMC), Vietnam to evaluate the changes to seasonal compound floods at the extreme level driven by both meteorological and oceanographic factors (inland rainfall and skew surge) under climate change. As the characteristics of flood in HCMC have a strong seasonal dependency, the temporal changes of the monthly maxima of both factors and their correlation are quantified by the framework before the underlying reasons are discussed. A well-calibrated hydrodynamic model TELEMAC-2D (Hervouet, 2007) is employed to generate flood inundation maps of both current and future scenarios associated with sea level rise in both dry and wet seasons. The results are further compared with the climate projection (RCP4.5 and 8.5 scenarios). Based on the proposed framework, this nonstationary compound flood modelling system is expected to be used by the National Centre for Hydro-Meteorological Forecasting (NCHMF) of Vietnam for prediction at the national level.

The remainder of this paper is organized as follows: Section 2 describes the development of the framework; The case study and results are described and discussed in Section 3 while concluding remarks on the framework and the case study are given in Section 4.

2. Technical description of the framework

Fig. 1 presents the framework we developed to analyze compound floods driven by both the hydrometeorological driver (e.g., monthly maximum rainfall, MMR) and oceanographic driver (e.g., monthly maximum skew surge, MMS) in view of both stationarity and non-stationarity, in turn, linked to climate change. It can be described as the four main steps which are further elaborated respectively in the following subsections.

2.1. Step 1 trend and correlation analysis

This step aims to detect whether the values of each flood driver, and their correlation structure change with other covariates, which will be the basis for copula parameterization. As the temporal nonstationarity of the drivers is the objective of the case study, time is chosen as the candidate covariate. The framework employs the Block Bootstrapping Mann-Kendall (BBS-MK) test (Kundzewicz and Robson, 2004, 2004n, 2004zand Bayazit, 2012) to detect monotonic changes in a series of data at the significance level of 0.05 (R Package 'modifiedmk' Version 1.6). In addition, the Kendall's tau and Spearman correlation alongside a Rolling window method are used to test the correlation between the series of data and its changes over time (De Winter et al., 2016; Zar, 2005). The correlation coefficients, i.e., τ and ρ, respectively, indicate the possible positive or negative correlation between the time series, while the corresponding p-values are compared with the critical values at the significance level of 0.05 to decide whether to reject the null hypothesis that no correlation exists. The Rolling window method is employed to use a variety of predefined widths of the window and move forward to the end of the data (Inoue et al., 2017), which is carried out following the three steps presented in Supplementary Text S1.

2.2. Step 2 modelling marginal distributions of the series of data

To increase the flexibility of the framework for fitting the best marginal distribution of each driver, several widely used types of them are chosen as the marginal distribution candidates, which includes the Generalized Extreme Value (GEV) distribution, Generalized Pareto distribution, Gamma distribution, Lognormal distribution and Exponential distribution. Following the outcomes from Step 1, as shown in Fig. 1, two assumptions are made:

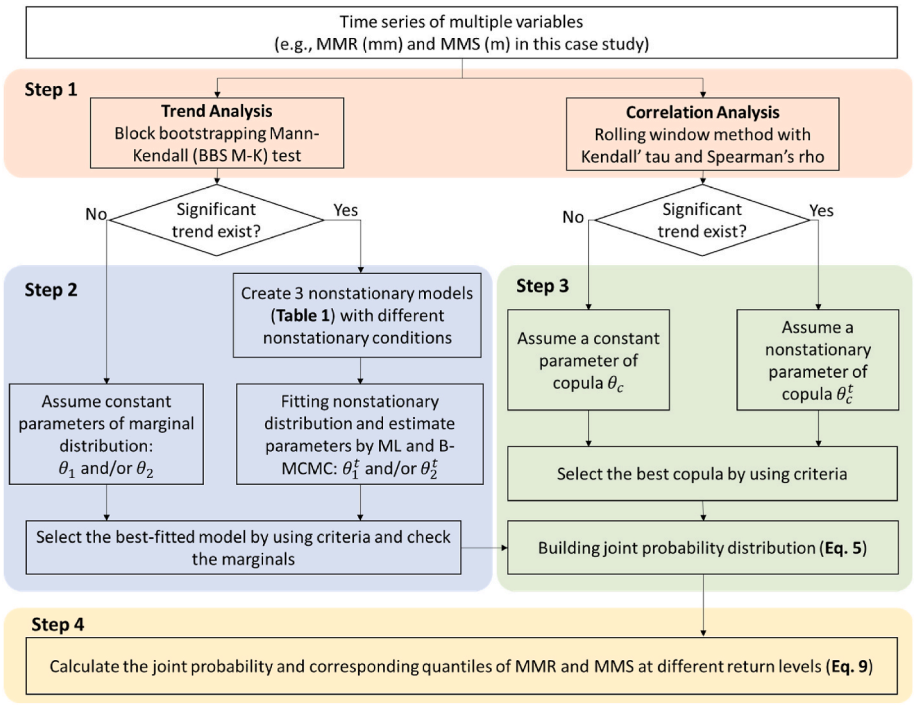

Fig. 1. The nonstationary framework of multivariate probability distribution analysis. MMR is the monthly maximum rainfall; MMS is the monthly maximum skew surge.

- of stationarity, where the parameters of the marginal distribution remain constant and independent and can be estimated by employing the Maximum Likelihood (ML) method.
- of nonstationarity, where certain parameters are assumed to be changing over time and can be estimated by using both the ML and the Bayesian Markov-Chain Monte-Carlo (B-MCMC) methods.

Table 1 presents a stationary and three nonstationary assumptions of these distributions. For those time series whose trend is determined to be insignificant, only the stationary assumption is applied, whereas both stationary and nonstationary distributions are applied. The best-fitted distribution is finally selected by evaluating the two criteria: Akaike's information criterion (AIC) and Bayesian information criterion (BIC); and the one with the minimum value indicates the best fitness (see Text S2).

Without losing generality, GEV distribution is exemplified below to demonstrate the procedure of building the stationary and nonstationary models. The same procedure is also followed in dealing with other types of distributions. The procedure of fitting a stationary model starts by defining the cumulative probability function F of the GEV:

$$F(x;\sigma,\mu,\xi)=\Pr(X\le x)=\exp\left[-\left(1+\xi\left(\frac{x-\mu}{\sigma}\right)\right)^{-\frac{1}{\xi}}\right]. \quad (1)$$

F is defined for $1+\xi(x-\mu)/\sigma>0, -\infty<\mu<\infty, \sigma>0$ and $-\infty<\xi<\infty$, where μ is the location parameter, σ is the scale parameter, and ξ is the shape parameter which defines the three types of distribution in the GEV family: type I when $\xi=0$, also known as the Gumbel distribution; types II and III are known as the Fréchet and the Weibull distributions, corresponding to $\xi>0$ and $\xi<0$, respectively. The ML method is employed to estimate these parameters by maximizing the likelihood function:

$$L(x;\boldsymbol{\theta})=\prod_{n=n_1}^{n_{1+N}} f(x;\boldsymbol{\theta})=\left(\frac{1}{\sigma}\left(1+\xi\left(\frac{x-\mu}{\sigma}\right)\right)^{-\frac{1}{\xi}-1}\exp\left(-\left(1+\xi\left(\frac{x-\mu}{\sigma}\right)\right)^{-1/\xi}\right)\right)^{N} \quad (2)$$

where n indicates the position from n_1 to n_{1+N} of the data series, N is the length of the time period and the parameter of the stationary model is denoted as $\boldsymbol{\theta}=(\sigma,\mu,\xi)$.

The nonstationary model is built when the data series show a significant trend. In this case, the nonstationary cumulative probability can be calculated as:

$$F_t(x;\sigma_t,\mu_t,\xi)=\exp\left[-\left(1+\xi\left(\frac{x-\mu_t}{\sigma_t}\right)\right)^{-\frac{1}{\xi}}\right]. \quad (3)$$

F_t follows the same form as the stationary one with an additional subscript t added to the location and scale parameters, which indicates that both parameters are time-dependent and controlled by several hyper-parameters, i.e., for MMS $\sigma_t=(\sigma_{S0},\sigma_{S1})$ and $\mu_t=(\mu_{S0},\mu_{S1})$, and for MMR $\sigma_t=(\sigma_{R0},\sigma_{R1})$ and $\mu_t=(\mu_{R0},\mu_{R1})$. The shape parameter, ξ_s and ξ_R, is assumed to be constant. Therefore, the parameters of nonstationary models can be denoted as $\boldsymbol{\theta}_t$ including $\boldsymbol{\theta}_S=(\sigma_{S0},\sigma_{S1},\mu_{S0},\mu_{S1},\xi_S)$ and $\boldsymbol{\theta}_R=(\sigma_{R0},\sigma_{R1},\mu_{R0},\mu_{R1},\xi_R)$.

Both ML and B-MCMC methods are used to estimate $\boldsymbol{\theta}_t$. The B-MCMC method makes use of Bayesian inference to estimate the posterior distribution of the time-varying parameters where $\boldsymbol{\theta}$ of the stationary model are used to define the initial prior values of the nonstationary model assuming a uniform distribution. The transformation from prior distribution to posterior distribution is done by multiplying its likelihood, which is given by (Rasmussen and Ghahramani, 2003):

$$p(\boldsymbol{\theta}|x,t)\propto p(\boldsymbol{\theta}|t)\times p(x|\boldsymbol{\theta},t)=p(\boldsymbol{\theta}|t)\times\prod_{t=1}^{N}p(x_t|\boldsymbol{\theta}_t,t) \quad (4)$$

where $p(x|\boldsymbol{\theta},t)\propto L(x;\boldsymbol{\theta},t)$ is the likelihood function and $p(\boldsymbol{\theta}|t)$ is the prior probability distribution of the parameters $\boldsymbol{\theta}$; t indicates the state. Numerical iterations for processing the posterior distribution are carried out by using MCMC simulation (Manly, 2018; Metropolis and Ulam, 1949; Murthy, 2004); more details can be found in Text S3. The final simulation results are compared with those estimated using the ML method.

Table 1
Stationary (S) and nonstationary (NS) candidate distributions for time series.

Distribution	Model	Description	Parameters ($\boldsymbol{\theta}$)
Generalized extreme value distribution	S	$F(x;\sigma,\mu,\xi)=\begin{cases}\exp\left[-\left(1+\xi\left(\frac{x-\mu}{\sigma}\right)\right)^{-1/\xi}\right], \xi\neq 0\\ \exp\left[-\exp\left(\frac{x-\mu}{\sigma}\right)\right], \xi=0\end{cases}$ where $1+\xi(x-\mu)/\sigma>0, -\infty<\mu<\infty, \sigma>0$ and $-\infty<\xi<\infty$.	$\boldsymbol{\theta}=\{\sigma,\mu,\xi\}$ where σ,μ,ξ are all constant.
	NS1	$F_t(x;\sigma,\mu_t,\xi)$	$\boldsymbol{\theta_t}=\{\mu_0,\mu_1,\sigma,\xi\}$ where $\mu_t=\mu_0+\mu_1\times t$ σ,ξ are constant
	NS2	$F_t(x;\sigma_t,\mu_t,\xi)$	$\boldsymbol{\theta_t}=\{\mu_0,\mu_1,\sigma_0,\sigma_1,\xi\}$ where $\mu_t=\mu_0+\mu_1\times t$ $\sigma_t=\sigma_0+\sigma_1\times t$ ξ is constant
	NS3	$F_t(x;\sigma_t,\mu_t,\xi)$	$\boldsymbol{\theta_t}=\{\mu_0,\mu_1,\sigma_0,\sigma_1,\xi\}$ where $\mu_t=\mu_0+\mu_1\times t$ $\sigma_t=\exp(\sigma_0+\sigma_1\times t)$ ξ is constant
Generalized Pareto distribution	S	$F(x;\sigma,\mu,\xi)=\begin{cases}1-\left(1+\xi\left(\frac{x-\mu}{\sigma}\right)\right)^{-1/\xi}, \xi\neq 0\\ 1-\exp\left(-\frac{x-\mu}{\sigma}\right), \xi=0\end{cases}$ where $x\geq\mu$ when $\xi\geq 0$ and $\mu\leq x\leq\mu-\sigma/\xi$ when $\xi<0$.	$\boldsymbol{\theta}=\{\sigma,\mu,\xi\}$ where σ,μ,ξ are all constant
	NS1	$F_t(x;\sigma,\mu_t,\xi)$	$\boldsymbol{\theta_t}=\{\mu_0,\mu_1,\sigma,\xi\}$ where $\mu_t=\mu_0+\mu_1\times t$ σ,ξ are constant
	NS2	$F_t(x;\sigma_t,\mu_t,\xi)$	$\boldsymbol{\theta_t}=\{\mu_0,\mu_1,\sigma_0,\sigma_1,\xi\}$ where $\mu_t=\mu_0+\mu_1\times t$ $\sigma_t=\sigma_0+\sigma_1\times t$ ξ is constant
	NS3	$F_t(x;\sigma_t,\mu_t,\xi)$	$\boldsymbol{\theta_t}=\{\mu_0,\mu_1,\sigma_0,\sigma_1,\xi\}$ where $\mu_t=\mu_0+\mu_1\times t$ $\sigma_t=\exp(\sigma_0+\sigma_1\times t)$ ξ is constant
Gamma distribution	S	$F(x;\sigma,\xi)=\frac{1}{\Gamma(\xi)}\gamma\left(k,\frac{x}{\sigma}\right)$ Where $x>0$, $\sigma>0,\xi>0$.	$\boldsymbol{\theta}=\{\sigma,\xi\}$ where σ,ξ are all constant
	NS1	$F_t(x;\sigma,\xi_t)$	$\boldsymbol{\theta_t}=\{\xi_0,\xi_1,\sigma\}$ where $\xi_t=\xi_0+\xi_1\times t$ σ is constant
	NS2	$F_t(x;\sigma_t,\xi_t)$	$\boldsymbol{\theta_t}=\{\xi_0,\xi_1,\sigma_0,\sigma_1\}$ where< $\xi_t=\xi_0+\xi_1\times t$ $\sigma_t=\sigma_0+\sigma_1\times t$
Lognormal distribution	S	$F(x;\sigma,\mu)=\varnothing\left(\frac{\ln x-\mu}{\sigma}\right)$ Where $\varnothing$ is the cumulative distribution function of the standard normal distribution.	$\boldsymbol{\theta}=\{\sigma,\mu\}$ where σ,μ are all constant
	NS1	$F_t(x;\sigma,\mu_t)$	$\boldsymbol{\theta_t}=\{\mu_0,\mu_1,\sigma\}$ where $\mu_t=\mu_0+\mu_1\times t$ σ are constant
	NS2	$F_t(x;\sigma_t,\mu_t)$	$\boldsymbol{\theta_t}=\{\mu_0,\mu_1,\sigma_0,\sigma_1\}$ where $\mu_t=\mu_0+\mu_1\times t$ $\sigma_t=\sigma_0+\sigma_1\times t$
	NS3	$F_t(x;\sigma_t,\mu_t)$	$\boldsymbol{\theta_t}=\{\mu_0,\mu_1,\sigma_0,\sigma_1,\xi\}$ where $\mu_t=\mu_0+\mu_1\times t$ $\sigma_t=\exp(\sigma_0+\sigma_1\times t)$
Exponential distribution	S	$F(x;\sigma)=\begin{cases}\frac{1}{\sigma}\exp\left(-\frac{x}{\sigma}\right), x>0\\ 0, x<0\end{cases}$ Where the scale parameter $\sigma=1/\lambda$ and $\lambda>0$ is the rate parameter of the exponential distribution.	$\boldsymbol{\theta}=\{\sigma\}$ where σ is constant
	NS2	$F_t(x;\sigma_t)$	$\boldsymbol{\theta_t}=\{\sigma_0,\sigma_1\}$ where $\sigma_t=\sigma_0+\sigma_1\times t$
	NS3	$F_t(x;\sigma_t)$	$\boldsymbol{\theta_t}=\{\sigma_0,\sigma_1\}$ where $\sigma_t=\exp(\sigma_0+\sigma_1\times t)$

Noted that μ, σ and ξ indicate location, scale and shape parameter of distribution respectively; $\boldsymbol{\theta}$ and $\boldsymbol{\theta_t}$ are symbols to indicate the parameters for each model needing to be estimated and the subscript t is used for indicating the nonstationary model; S is short for "stationarity" case and NS1, NS2 and NS3 indicate three "nonstationarity" cases.

2.3. Step 3 building copulas and calculating the joint probability

Let J denote the joint cumulative distribution of the two series of data, and C denote the copula parameterized by θ_C. Then, the basic joint probability can be calculated by:

$$J(x_S, x_R|\theta_C) = C(F_1(x_1|\boldsymbol{\theta_1}), F_2(x_2|\boldsymbol{\theta_2})|\theta_C) = C(u, v|\theta_C) \quad (5)$$

where F_1 and F_2 indicate the marginal cumulative probability function of the two series of data x_1 (in the case study, MMS) and x_2 (MMR) with their estimated parameters $\boldsymbol{\theta_1}$ and $\boldsymbol{\theta_2}$ respectively, and θ_C indicates the set of parameters of the copula. u and v are the marginal probabilities of F_1 and F_2 in the unit hypercube with uniform marginal distributions $U(0,1)$. According to the trend analysis of the individual data series and their mutual correlation structure, four contexts are relevant in this framework:

- Both marginal distributions ($\boldsymbol{\theta}$) are stationary, and the correlation structure (θ_C) is stationary.
- Both marginal distributions ($\boldsymbol{\theta}$) are stationary, while the correlation structure (θ_C^t) is nonstationary.
- At least one of the marginal distributions ($\boldsymbol{\theta_t}$) is nonstationary, while the correlation structure (θ_C) is stationary.
- At least one of the marginal distributions ($\boldsymbol{\theta_t}$) is nonstationary, while the correlation structure (θ_C) is nonstationary.

In this framework, several widely-used one-parameter copulas are selected as the candidates to characterize the dependence structure between two series of data, namely, Gaussian, Clayton, Frank, Gumbel, Joe, Plackett and Raftery copulas whose parameter θ_C is estimated by using both the local optimization method and MCMC method. However, if there is no significant correlation identified, an independent copula is also involved by simply reducing to the form of the product of two marginal probabilities.

For the nonstationary copula whose parameter varies over time, we assume that the copula is controlled by a θ_C^t with two hyper-parameters θ_{C0} and θ_{C1} and the joint cumulative distribution can be written as the follows and estimated by modifying the MvCAT toolbox (Sadegh et al., 2017) to incorporate the nonstationary terms (see the details in Text S4):

$$J_t(x_{1t}, x_{2t}|\theta_C^t) = C(F_{1t}(x_{1t}|\boldsymbol{\theta_{1t}}), F_{2t}(x_{2(t)}|\boldsymbol{\theta_{2t}})|\theta_C^t) = C(u_t, v_t|\theta_C^t) \quad (6a)$$

$$\theta_C^t = \theta_{C0} + \theta_{C1} \times t \quad (6b)$$

where $\boldsymbol{\theta_{1t}}$ and $\boldsymbol{\theta_{2t}}$ indicate the time-varying parameters of the two marginal distributions shown in Table 2 and u_t, v_t are the nonstationary marginal probabilities converting in the uniform U [0,1]. These parameters are estimated by the B-MCMC method with the posterior joint distribution calculated as (Ausin et al., 2010):

$$p(\varnothing|x_{1t}, x_{2t}) \propto p(\varnothing|t) \times \prod_{t=1}^{N} p(x_{1t}, x_{2t}|\varnothing, t) \quad (7)$$

where $p(x_{1t}, x_{2t}|\varnothing, t) = c(F_{1t}(x_{1t}|\boldsymbol{\theta_{1t}}), F_{2t}(x_{2(t)}|\boldsymbol{\theta_{2t}})|\theta_C^t) \times f_{1t}(x_{1t}|\boldsymbol{\theta_{1t}}) \times f_{2t}(x_{2t}|\boldsymbol{\theta_{2t}})$ is the copula density function, f_{1t} and f_{2t} are the marginal probability density functions and the parameters of the joint posterior are $\varnothing = (\mu_{S0}, \mu_{S1}, \sigma_{S0}, \sigma_{S1}, \xi_S, \mu_{R0}, \mu_{R1}, \sigma_{R0}, \sigma_{R1}, \xi_2, \theta_{C0}, \theta_{C1})$. $p(\varnothing|t)$ is the prior distribution of the parameters $\varnothing$ and according to the prior knowledge for which we assume a uniform distribution for all parameters with reference to their stationary estimations within the maximum and minimum limits subject to copula types. To reduce the computing time, the nonstationary marginal parameters are firstly estimated by applying step 2 before being transformed into u_t and v_t. The MCMC in this step is only used to estimate the time-varying copula parameter:

$$p(\theta_C^t|u_t, v_t) \propto p(\theta_C^t|t) \times \prod_{t=1}^{N} c(u_t, v_t|\theta_C^t, t) \quad (8)$$

Finally, the best copula is selected by evaluating the goodness of fit measure AIC and BIC.

2.4. Step 4 generating the quantiles

The final step is to calculate the corresponding quantiles of the joint exceedance probability with a given probability of p, where the stationary context will lead to a single quantile and the nonstationary

Table 2
Test and estimation results of monthly maximum rainfall (MMR) and skew surge (MMS) in HCMC.

Month	Time series	BBS-MK test		Correlation test (with all datasets)				Best-fitted marginal distribution		Best-fitted copula	
		Kendall's tau	*p*-value	τ	*p*-value	ρ	*p*-value	Type	$\boldsymbol{\theta}$	Copula	θ_C
Jan	MMS	0.34	**0.003**	0.10	0.379	0.13	0.427	GEV	S	Independence	S
	MMR	0.11	0.326					Gamma	S		
Feb	MMS	0.45	**0.000**	0.09	0.445	0.14	0.403	GEV	S	Independence	S
	MMR	0.08	0.491					Gamma	S		
Mar	MMS	0.35	**0.002**	0.21	0.062	0.34	**0.038**	GEV	S	Gaussian	NS
	MMR	0.17	0.137					Gamma	S		
Apr	MMS	0.38	**0.001**	0.27	**0.017**	0.36	**0.026**	GEV	NS1	Clayton	NS
	MMR	0.47	**0.000**					GEV	NS1		
May	MMS	0.16	0.167	0.02	0.860	0.04	0.823	GEV	S	Independence	S
	MMR	−0.01	0.940					GEV	S		
Jun	MMS	0.41	**0.001**	−0.08	0.490	−0.10	0.559	LogN	S	Plackett	S
	MMR	−0.08	0.497					GEV	S		
Jul	MMS	0.49	**0.000**	−0.08	0.469	−0.10	0.562	GEV	S	Independence	S
	MMR	−0.06	0.615					LogN	S		
Aug	MMS	0.49	**0.000**	0.09	0.453	0.14	0.392	GEV	S	Raftery	S
	MMR	−0.04	0.763					LogN	S		
Sep	MMS	0.44	**0.000**	0.07	0.532	0.10	0.568	GEV	S	Raftery	S
	MMR	0.20	0.083					GEV	S		
Oct	MMS	0.35	**0.002**	0.16	0.168	0.24	0.140	GEV	S	Joe	S
	MMR	0.23	**0.039**					GEV	NS1		
Nov	MMS	0.25	**0.031**	0.13	0.257	0.18	0.276	GEV	S	Joe	S
	MMR	0.22	**0.050**					GEV	NS3		
Dec	MMS	0.38	**0.001**	0.21	0.059	0.29	0.075	GEV	S	Raftery	S
	MMR	0.22	0.053					GEV	S		

Noted that GEV, Gamma, LogN are short for "Generalized extreme value distribution", "Gamma distribution" and "Log-normal distribution" respectively while S indicates stationary (constant) assumption and NS indicates the nonstationary (time-varying) assumption.

context will obtain a series of quantiles changing over the covariate (i.e., time in the study):

$$Q(p) = \left(x_1 = {F_{1t}}^{-1}\left(u|\boldsymbol{\theta}_1^t\right), x_2 = {F_{2t}}^{-1}\left(v|\boldsymbol{\theta}_2^t\right)\right) \quad (9)$$

where $p = C_t(u, v|\theta_C^t)$ and t indicates that the parameters or variables are changing over time. If the context is stationary and the two variables are independent, $Q(p)$ can be simply calculated by inverting the marginal distributions, i.e., $x_1 = {F_1}^{-1}(u|\boldsymbol{\theta}_1)$ and $x_2 = {F_2}^{-1}(v|\boldsymbol{\theta}_2)$.

There are several approaches to selecting the cases of combination of the corresponding values of two variables and the most used of which is to get the most likely combined with the highest joint density level (Sadegh et al., 2018; Salvadori et al., 2014). Fig. 2 exemplifies all quantile curves corresponding to the probability from $p = 0.01$ to $p = 0.99$. The horizontal x-axis and vertical y-axis are two marginal variables where all the combinations of these two variables along the same curve correspond to the same p. The most likely scenarios method is to peak up the combination where the joint density of this quantile curve is the highest. The z-axis of Fig. 2 indicates the joint density level uniformed to the range of (0,1) and the blue circles indicate the location where the density level is 1.0 while the corresponding combination of MMS and MMR is the most likely one. The other commonly used approach is to sample all the combinations instead of selecting only one, however, this means the scenario selection has stochasticity which requires to be further analysed. Therefore, the most likely scenario approach is applied in the framework.

3. Result and discussion

3.1. Study domain and data analysis

As a major economic centre of Vietnam, Ho Chi Minh City (HCMC) is located in the downstream reach of the Saigon and Dong Nai rivers (Fig. 3a) with nearly 10 million inhabitants, contributing more than 20% of the GDP of the nation (Hallegatte et al., 2013; Kontgis et al., 2014). Yet, due to its geographical location and the ageing infrastructure, the city is vulnerable to frequent floods resulting from concurrent intense rainfall and strong surges, commonly known as compound flooding (Binh et al., 2019; Nguyen et al., 2019; Vachaud et al., 2019). The rising sea levels have been driving the threats of compound flooding

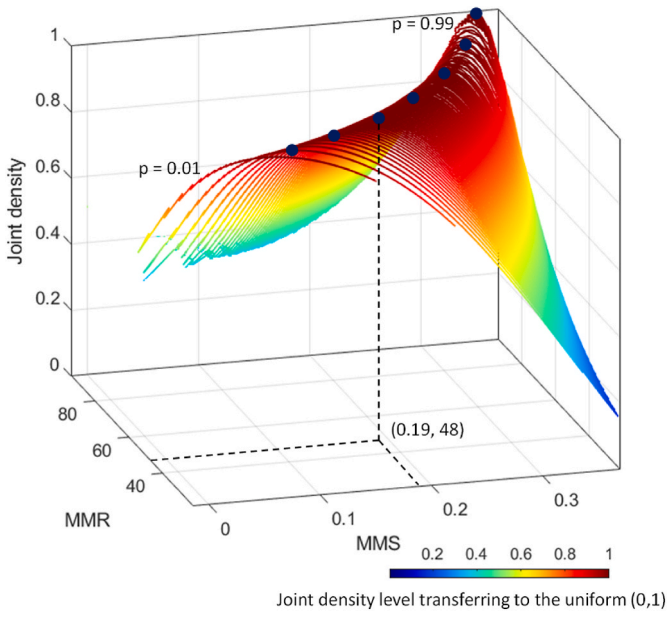

Fig. 2. Joint density level of quantile curves corresponding to the probability from 0.01 to 0.99.

to an even higher level with further complications. Therefore, it is imperative to apply a quantitative nonstationary framework to evaluate compound floods taking climate change into account.

Two observed datasets are applied in this study, i.e., daily rainfall collected from six rain gauges in the vicinity of HCMC and hourly sea level at the estuary of the Vung Tau water level gauge (see Fig. 3a). Both datasets cover a period of 38 years from 01/01/1980 to 31/12/2017 and are provided by the Southern Regional Hydrometeorological Center, Vietnam. The gauged rainfall is firstly converted to areal rainfall by applying the Thiessen polygon method and the surge is calculated as the difference between the highest observed sea level and high tide within a tidal period, where the details of data processing are given in Couasnon et al. (2022). Finally, the monthly maxima from the series of daily areal rainfall (henceforth, MMR) and of daily surge (henceforth, MMS) are extracted before being used to estimate the dependence and risk, again, in a seasonal fashion. Boxplots of MMS and MMR are depicted in Fig. 3b where MMS shows much fewer variations compared with MMR which has a strong dry-wet season variation. As to the seasonal variation, the extreme cases in MMR (i.e., daily rainfall higher than 90 mm) occur frequently in the wet season (i.e., August, September, October); in comparison, the extreme cases of skew surge appear mainly in the three dry months (February, March, April) and one wet month (July which has the largest deviation (around 0.4m) from the 5th to 95th percentiles).

3.2. Trend and time-varying correlation of MMS and MMR

The first step in the application of the framework (see Fig. 1) is to detect whether the series of MMS and MMR and their correlation structure vary with time. This is achieved by using the Block Bootstrapping Mann-Kendall test, and the Rolling Window combined with Kendall and Spearman test respectively. The results (see Table 2) show that MMS of all months but May were detected to be increasing during the 38-year period at a significance level of 0.05 and there is a small difference in the magnitude of these positive trends between the dry and wet seasons of HCMC. For MMR, there are only one month of dry season and two out of the eight months of wet season (May–November), i.e., April, October and November showing a significant trend over time. Regarding the correlation between MMS and MMR, the two dry months March and April witnessed a significant, positive correlation and such correlation varies with time (see Fig. 4).

The left panel of Fig. 4 presents the correlation test statistics (τ and ρ, left axis) and the corresponding p-values (right axis) which change over time with a window width of 30 years. The correlation between MMS and MMR in March (Fig. 4a) weakens continuously initially before getting strengthened during the period around 1983–2012 to 1986–2015 and then decreases again in the final periods of 1987–2016 and 1988–2017. In April (Fig. 4b), the correlation in the first period (1980–2009) is strong and becomes weak in the periods afterwards. As the correlation calculation can be sensitive to the selection of the time window width, different width setups are used to test the consistency of the results as presented in Fig. S1, which shows a general good consistency across the results.

It is rather intriguing to see such a stronger and time-varying correlation between MMS and MMR in March and April. One of the most plausible reasons is that both MMS and MMR are directly affected by the easterly wind flow. This flow blows perpendicularly toward the coastal area in the South of Vietnam only in these two months such that it strongly stresses the surface layer water into the mainland. This leads to a higher surge as presented in the right panel of Fig. 4. In addition, rainfall in these two months comes mainly from the perturbation and moisture from the easterly wind that also facilitates convection. However, in other dry months, the wind gradually moves from easterly to north-easterly and parallel to the coastal area; while in wet months, this easterly component retreats to the middle and the northeast of Vietnam's East Sea when the rainfall events in Vietnam are dominated by the summer monsoon from the Bay of Bengal.

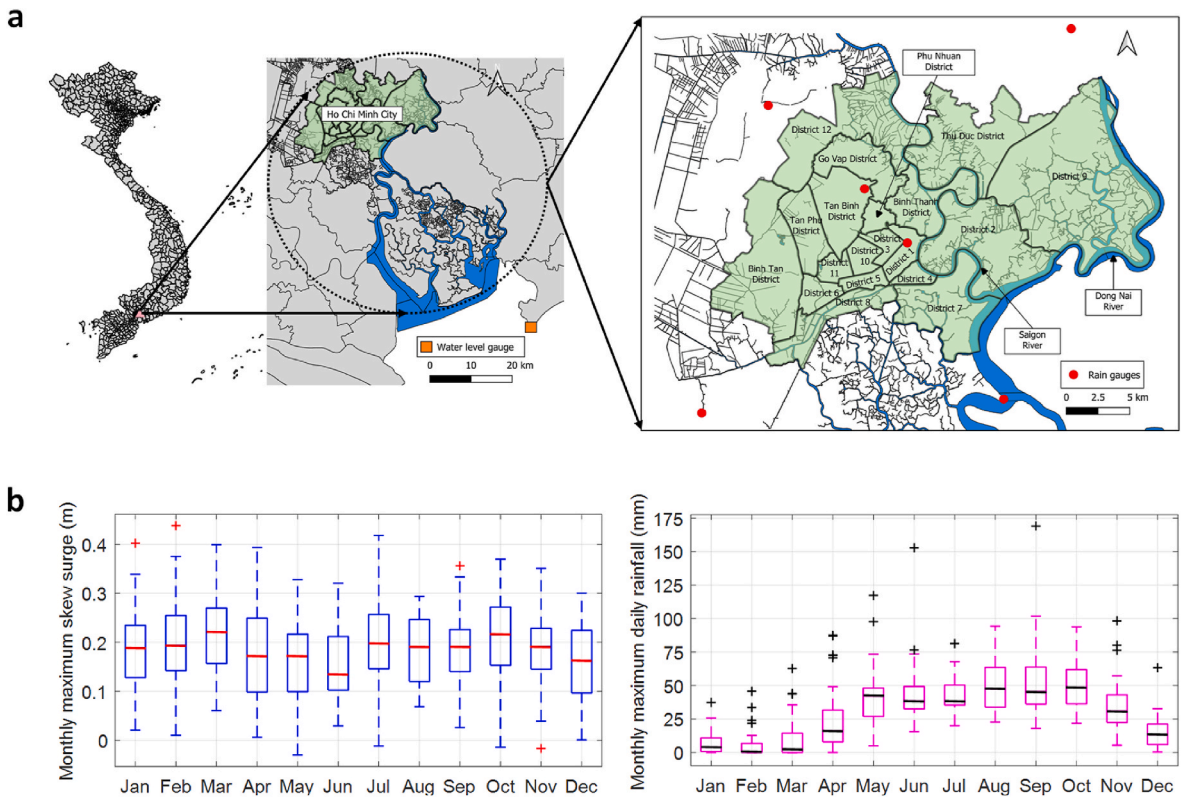

Fig. 3. (a) The study area (Ho Chi Minh City) where the six rain gauges for collecting the daily rainfall over the city centre are denoted by red circles and a water level gauge by a yellow rectangle and (b) boxplots of monthly maximum time series of surge and rainfall (1980–2017). In each box, the central mark indicates the median, and the bottom and top edges of the box indicate the 25th and 75th percentiles, respectively, and the outliers are indicated by '+'.

3.3. Stationary and nonstationary joint probability analysis

Following the rest three steps (steps 2–4 of Fig. 1) of the framework, the joint probability of MMS and MMR is estimated using the most suitable candidates of marginal distributions and copulas. For the case that both marginal distribution and copula can be best fitted by stationary models, e.g., July, the result is shown to be the same as that from the traditional multivariate probability analysis. However, when either marginals or copula is best fitted nonstationarily, the features of quantiles corresponding to joint exceedance probabilities are different. For example, October is best estimated by a time-varying distribution of MMR but the correlation structure does change significantly over time. Fig. 5 demonstrates how the quantile curves change over time with only a single distribution varying with time where it can be observed that the time-varying marginal distribution can only cause an upward or downward movement of the quantile curves at each exceedance probability, but the shape of these curves remains unchanged. However, the shape of the quantile curves can be affected by a time-varying copula, which is demonstrated by the case of March whose marginal distributions are constant, but the correlation structure varies with time. The results show that the changes in shapes are more significant in the middle than in the tails. Furthermore, April has both time-varying marginals and correlation structure and the results show that the quantile curves twist over time where such change is translational at the lower tail of quantile curves (e.g., the combination of the same skew surge with higher rainfall) while at the middle, the angle of the curves shrinks (e.g., the combination of both lower skew surge and rainfall). The fitting results are presented in Tables S1 and S2 and more details about the parameter estimation and model selection are given in Text S5.

3.4. Nonstationary compound flood simulations in HCMC

To simulate the changes of compound flooding in HCMC that may be due to human factors or climate change, while mitigating the computational overheads, we selected two typical months for simulations, i.e., March and October that represent the dry and wet seasons respectively in this study. Flood inundation maps are generated using the designed pair of high rainfall and skew surge at the return level of 1-in-50-years which are chosen based on the quantile curves presented in March and October of Fig. 5 by using the most likely scenario method. The designed pair is then used to drive the calibrated TELEMAC-2D model (see Text S6) by applying it with a 24-h profile.

After examining the historical records over the 38-year study period (see Text S7), the maximum skew surge in most situations occurs near the second peak of the tide (around 63% happened at the second peak and in 80% of situations, there is no time difference between the water level peak and tide peak). Therefore, the designed skew surge is added to the second tide peak and then interpolated to the other time points (24 h) to generate the profile of the water level. To consider the climate change impact, sea-level rise (SLR) is also added to water level to set the lower boundary condition of the TELEMAC-2D model simulation. The values of SLR are provided by the Ministry of Natural Resources and Environment, Vietnam, i.e., 0.12 m for 2020 and 0.33 m for 2050 relative to the period of 1980–1999 of high CO_2 emission (Pham, 2009).

The block rainfall value is distributed temporally using a 3-h profile with reference to the designed hyetograph (an example displayed in Fig. S5) based on the extreme rainfall analysis conducted in HCMC (Couasnon et al., 2022; Scussolini et al., 2017). Besides, to obtain the worst compound floods, the starting time of the rainfall event is experimentally set, as described in detail in Text S7, and finally defined as about 2 h before the water level peak is observed in the city center, i.e., the Phu An station, in the study area for each TELEMAC-2D simulation.

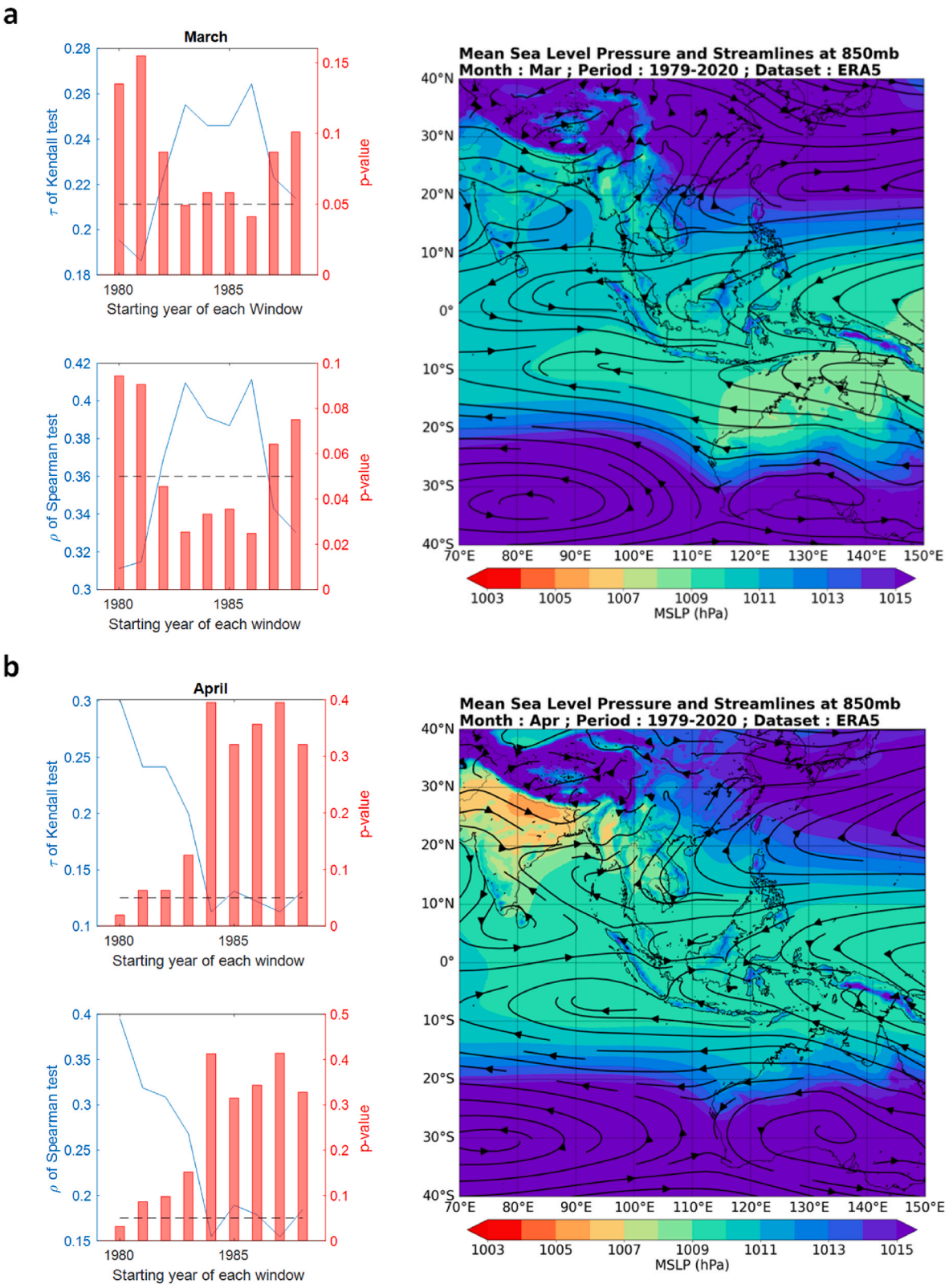

Fig. 4. Trend analysis of the correlation structure between MMS and MMR in (a) March and (b) April where the correlation coefficients τ of Kendall test and ρ of Spearman test are depicted by blue curves and the p-values are indicated by red bars with the significance level (0.05) is shown in dashed black line; the mean sea level pressure and wind velocity at 850 mb for (a) March and (b) April averaged from 1979 to 2020 using the ERA5 dataset (ECMWF, 2018).

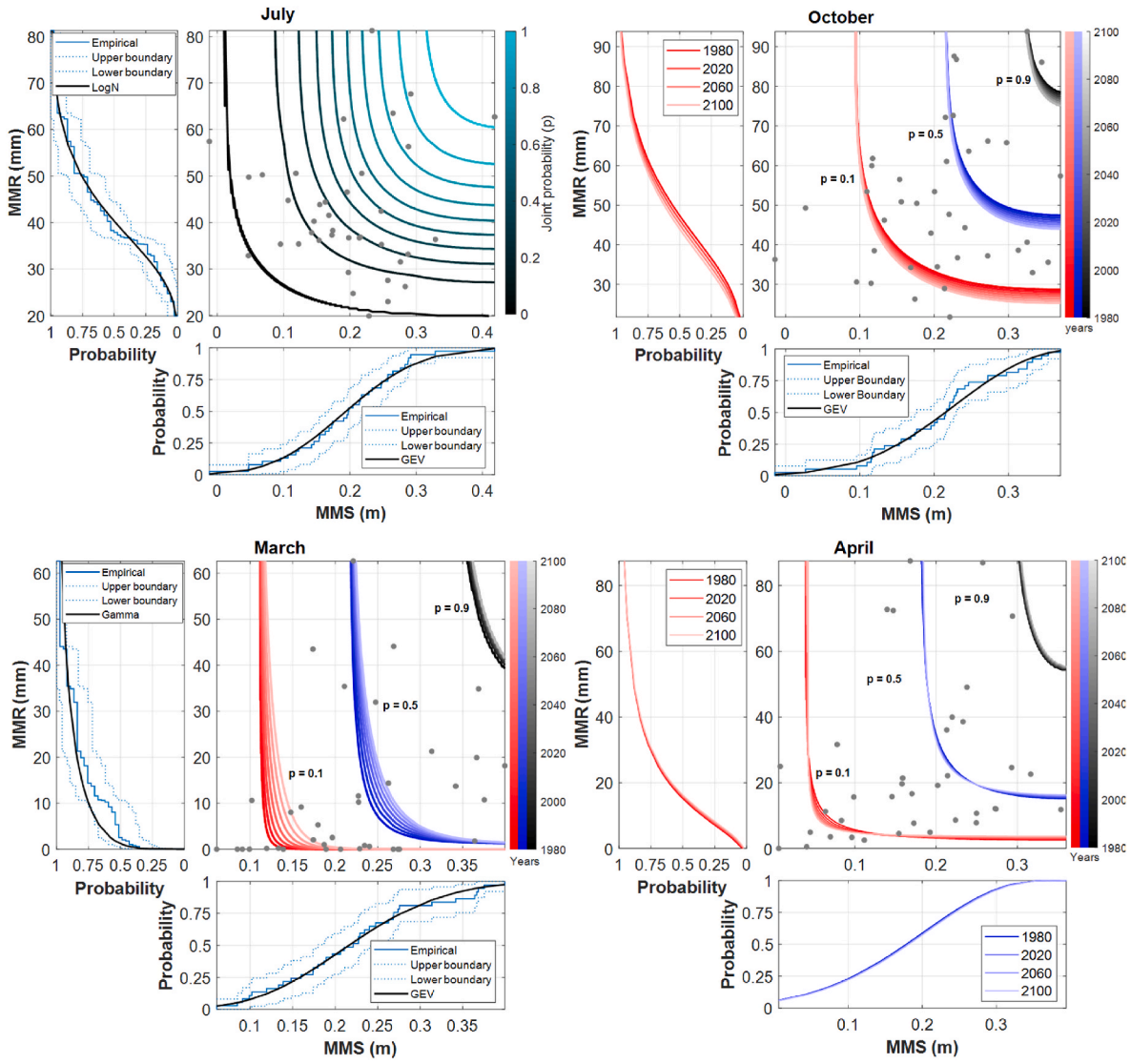

Fig. 5. Quantiles corresponding to different joint cumulative probabilities (p = 0.1, 0.5 and 0.9) of the monthly maximum skew surge and rainfall in the selected four months where the best-fitted distributions of the two marginals (MMS and MMR) are shown in the left and lower panels of each sub-figure respectively: when the best-fitted distribution is stationary, the comparison between the empirical and best-fitted distribution is shown while it is nonstationary, only the best-fitted distribution is plotted and colour of curves indicates the changes over time (year).

To compare with what would have been produced following the traditional approach, i.e., that does not consider the nonstationarity nor climate change, we also generated the stationary cases for the two months, i.e., by re-fitting the marginal distributions and copula with constant parameters. Simulations of the 1-in-50-year compound flood using the traditional approach (stationary simulations) are then compared with those using the proposed nonstationary framework (nonstationary simulations), as seen in Fig. 6a and b. The nonstationary framework is also used to simulate the future 2050 scenario and compare it with the current (2020) scenario to reveal the possible changes (Fig. 6c).

It can be observed that floods have more impact in the eastern regions of HCMC, especially in the confluent area of the Saigon and Dong Nai Rivers (southeast). Regarding the inundation areas simulated using the traditional stationary model (the top panel of Fig. 6a), floods are mainly driven by the inland rainfall and appear more severe in October over the northeast and away from the main river channels, which is due to the fact that the wet season receives more rainwater than the dry one. However, over the regions near rivers, e.g., the south part, the difference is small where flood water in March is even deeper than in October. This is because the surge in March is higher than in October although higher rainfall makes up the surge gap.

To compare the traditional approach with the proposed nonstationary simulation, we calculated the difference in flood depth between the stationary case and nonstationary for the current scenario 2020 (Fig. 6b). Most regions in both months, especially those over the southeast and north are underestimated by the stationary simulation when referring to the flooded areas and magnitude compared with the scenario 2020 simulated by the nonstationary framework. In March, higher rainfall and slightly lower skew surge are estimated, as indicated by the nonstationary correlation between them. The consequence is that in the west and northeast, where floods are mainly driven by rainfall, the estimated flood by the nonstationary framework is higher, and over the eastern regions near the Dong Nai River, it is even higher due to the increased rainfall and sea level rise making up for the decrease of skew surge. In October, however, the underestimation is not as significant and there is very little difference in the flooded regions mainly driven by rainfall whose average level is expected to decrease by the nonstationary framework. The correlation between the rainfall and surge is not as significant nor does it change over time. Therefore, the underestimation

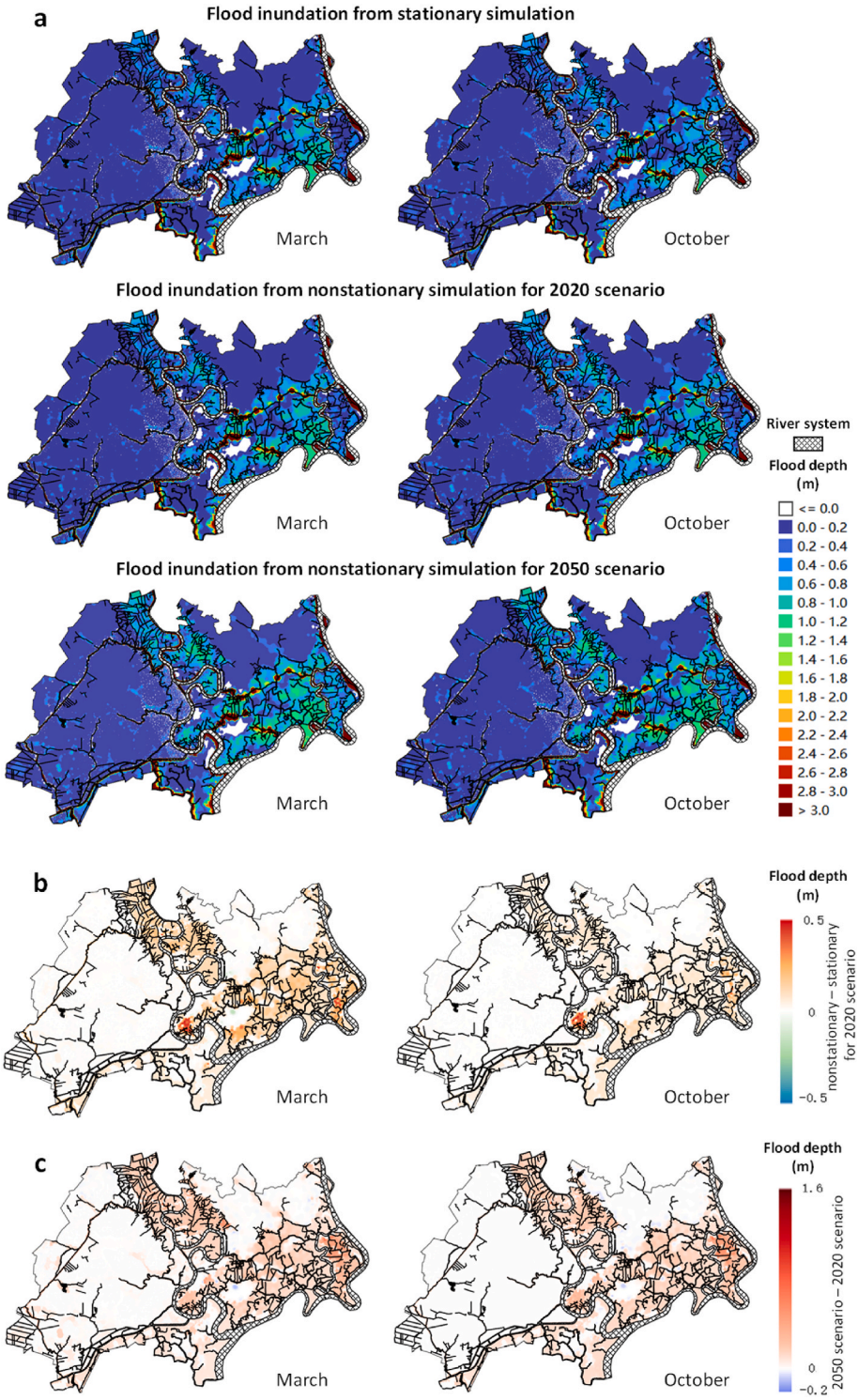

Fig. 6. (a) Flood inundation maps simulated using both the stationary model and nonstationary framework for the two scenarios (current: 2020 and future: 2050) in March and October; (b) the difference of nonstationary minus stationary for current scenario 2020 and (c) the difference between nonstationary for current and future scenario due to climate change.

by the stationary model can be attributed only to sea level rise due to climate change.

To reveal the temporal change of compound flood simulated by the nonstationary framework where the future case is generated by nonstationary extrapolation, we also generated the difference map between the current and future scenarios (see Fig. 6c) and further compared it with the regional climate simulations to investigate whether the simulated tendency is consistent. Several regional climate simulations show an overall decreasing annual rainfall total with a significant increase in consecutive dry days over Vietnam that has the potential to be drier by the end of this century (2081–2 100). However, the intensity and frequency of annual rainfall extremes are projected to increase (Myhre et al., 2019; Tangang et al., 2020; Trinh-Tuan et al., 2019). This finding agrees with our simulation that the flood driven by extreme rainfall and skew surge is expected to be higher (i.e., in the reddish regions in Fig. 6c while October has an even darker red colour).

The intensity of rainfall extremes in March shows an increase in our simulation which is in line with the projected increasing tendency under the RCP4.5 and RCP8.5 over Indochina including south Vietnam during March-April-May (Tangang et al., 2020). In October, rainfall at the average level is estimated to decrease, which is in line with the projected drying tendency over south Vietnam under the RCP8.5 during September-October-November-December (Trinh-Tuan et al., 2019). This is also revealed in the case of November where the rainfall estimated from the nonstationary framework increases at extreme frequency level but a slight decrease at the average level (see Table S1).

Besides, the time-varying correlation between the rainfall and skew surge can as well affect the frequency and magnitude of the compound floods in this low-lying area, e.g., March shows a nonstationary correlation structure, resulting in a combination of increased rainfall extremes and a slightly decreased high surge. Thus, the dry month of March is expected to get more floods triggered by rainfall extremes. These findings underpin the importance of incorporating nonstationarity into compound flood estimation because not only the drivers per se may change alongside the climate change, but their correlation can also vary due to many implicit factors which need further investigation. In Vietnam, although regional climate projection presents a drier tendency and less rainwater may be received in the future, it is important to focus on the floods driven by compound factors whose average values may decrease but the extreme level can increase.

4. Conclusion

This paper presents the seasonal changes of coastal compound floods in Ho Chi Minh City (HCMC) of Vietnam, which are driven by two nonstationary drivers (i.e., high rainfall and skew surge) and their time-varying interactions. To help the investigation, we developed a nonstationary multivariate modelling framework for quantifying the changes from the current to future cases (represented by 2020 and 2050) at the extreme level (i.e., 1-in-50-year), and further generated inundation maps using a well-calibrated hydrodynamic model TELEMAC-2D. The results are compared with the traditional analysis and regional climate projections. Several points can be drawn from our study:

1) The correlation between the monthly rainfall maxima and skew surges is independent except in March and April which are likely due to the direct effect of the easterly wind flow perpendicularly toward the coastal area in south Vietnam. The correlation in March becomes more significant in the last 10 years of the study period while in April it becomes less significant.
2) The series of monthly maximum rainfall in October and November (the wet season) have been changing over time and their distribution can be best fitted by the nonstationary generalized extreme value (GEV) model where the average rainfall is slightly decreased but the frequency of extremes is increased (especially in November).
3) The simulation results of the HCMC case study show that the traditional stationary approach underestimates the compound flood depth in current (2020) scenarios.
4) Compound flood simulated by the proposed nonstationary framework agrees with climate change estimated by the regional climate projections. March as a month of dry season, is expected to get more floods triggered by increased intensity and frequency of rainfall extremes whose magnitude is similar to the wet month of October, which is in line with the climate projection under the RCP4.5 and RCP 8.5 scenarios, although the dry spell duration is expected to increase and the annual rainfall total to decrease in Vietnam which can be reflected by a decreasing average level of rainfall in wet season in this study.

The nonstationary framework we developed offers flexibility in modelling complex compound extremes as far as the possible combinations of stationary and nonstationary marginals and their interactions are concerned. Besides, this paper presents the first application to evaluating compound flooding driven by extreme rainfall and skew surge from the perspective of nonstationarity in HCMC. Other low-lying coastal cities and countries may also confront a similar predicament where a comprehensive regional risk assessment of the compound flooding potential is currently missing. This modelling framework, with the flexibility it has, can find its many use cases in this regard.

The study also underpins that climate change can affect not only the hydrometeorological or oceanographic extremes per se but also their interaction which tends to become either more correlated or independent. As far as managing compound flood risk is concerned, relevant authorities should carefully consider such consequences arising from climate change and evaluate their current strategies that may have been historically produced from a stationary perspective.

Further work is recommended to investigate compound floods and the correlation between rainfall and surge with longer-term observations which are likely to make the conclusions more robust. As to the multivariate nonstationary framework, more copulas and types of distribution candidates can be involved alongside uncertainty quantifications. Apparently, linking climate model projections into the framework will be another important and challenging area to explore.

Author statement

Conceptualization: Han Wang, Yunqing Xuan, and Dominic E. Reeve; Methodology: Han Wang and Yunqing Xuan; Modelling: Thi Van Thu Tran; Software: Han Wang; Validation: Thi Van Thu Tran, Han Wang, and Hong Quan Nguye; Investigation: Linh Nhat Luu; Data Curation: Anaïs Couasnon, Thi Van Thu Tran, and Han Wang; Writing - Original Draft: Han Wang, Anaïs Couasnon, Thi Van Thu Tran, Paolo Scussolini and Linh Nhat Luu; Writing - Review & Editing: Han Wang, Yunqing Xuan, and Dominic E. Reeve; Supervision: Yunqing Xuan; Project administration: Yunqing Xuan, Anaïs Couasnon, Paolo Scussolini, and Hong Quan Nguyen; Funding acquisition: Yunqing Xuan.

Declaration of competing interest

The authors declare that they have no known competing financial interests or personal relationships that could have appeared to influence the work reported in this paper.

Data availability

the data are available on GitHub (doi:10.5281/zenodo.5763288), which has been published in https://doi.org/10.1029/2021WR030002

Acknowledgement

This work was jointly supported by the Academy of Medical Sciences, Grant Ref: GCRFNGR4_1165; Swansea University and HEFCW GCRF Grant Ref: RIG1032-114; Dutch Research Council (NWO) (VIDI grant No. 016.161.324; and grant No. ALWOP.164). The authors would like to thank the Southern Regional Hydro-meteorological Center for providing the time series at the rainfall and sea level gauges via the Center of Water Management and Climate Change in HCMC, Vietnam. And the data used to produce the results presented in this study (the time series of rainfall, daily high tide, skew surge) are available on GitHub (https://doi.org/10.5281/zenodo.5763288), which has been published in https://doi.org/10.1029/2021WR030002. The ERA5 data used to analyze the underlying reasons for the correlation in all months are available at https://doi.org/10.1002/qj.3803. The analysis of the data and all simulations are available on GitHub at https://github.com/wanghan924/HMCM_compound-flood (https://doi.org/10.5281/zenodo.7310411).

Appendix A. Supplementary data

Supplementary data to this article can be found online at https://doi.org/10.1016/j.coastaleng.2023.104330.

References

Ausin, M.C., Lopes, H.F., Analysis, D., 2010. Time-varying joint distribution through copulas. Comput. Stat. Data Anal. 54 (11), 2383–2399. https://doi.org/10.1016/j.csda.2009.03.008.

Bermúdez, M., Farfán, J., Willems, P., Cea, L., 2021. Assessing the effects of climate change on compound flooding in coastal river areas. Water Resour. Res. 57 (10), e2020WR029321 https://doi.org/10.1029/2020WR029321.

Bevacqua, E., Vousdoukas, M.I., Zappa, G., Hodges, K., Shepherd, T.G., Maraun, D., Mentaschi, L., Feyen, L., 2020. More meteorological events that drive compound coastal flooding are projected under climate change. Commun. Earth Environ. 1 (47), 1–11. https://doi.org/10.1038/s43247-020-00044-z.

Binh, L.T.H., Umamahesh, N., Rathnam, E.V., 2019. High-resolution flood hazard mapping based on nonstationary frequency analysis: case study of Ho Chi Minh City. Vietnam. Hydrol. Sci. J. 64 (3), 318–335. https://doi.org/10.1080/02626667.2019.1581363.

Corbella, S., Stretch, D.D., 2013. Simulating a multivariate sea storm using Archimedean copulas. Coast. Eng. 76, 68–78. https://doi.org/10.1016/j.coastaleng.2013.01.011.

Couasnon, A., Scussolini, P., Tran, T., Eilander, D., Muis, S., Wang, H., Keesom, J., Dullaart, J., Xuan, Y., Nguyen, H., 2022. A flood risk framework capturing the seasonality of and dependence between rainfall and sea levels—an application to Ho Chi Minh city. Vietnam. Water Resour. Res. 58 (2), e2021WR030002 https://doi.org/10.1029/2021WR030002.

Davies, G., Callaghan, D.P., Gravois, U., Jiang, W., Hanslow, D., Nichol, S., Baldock, T., 2017. Improved treatment of nonstationary conditions and uncertainties in probabilistic models of storm wave climate. Coast. Eng. 127, 1–19. https://doi.org/10.1016/j.coastaleng.2017.06.005.

De Winter, J.C., Gosling, S.D., Potter, J., 2016. Comparing the Pearson and Spearman correlation coefficients across distributions and sample sizes: a tutorial using simulations and empirical data. Psychol. Methods 21 (3), 273. https://doi.org/10.1037/met0000079.

ECMWF (European Centre for Medium-Range Weather Forecasts), 2018. ERA5 Hourly Data on Pressure Levels from 1959 to Present. Copernicus Climate Change Service (C3S) Climate Data Store (CDS). https://doi.org/10.24381/cds.bd0915c6 (Accessed on 20 Jan 2023).

Edmonds, D.A., Caldwell, R.L., Brondizio, E.S., Siani, S.M., 2020. Coastal flooding will disproportionately impact people on river deltas. Nat. Commun. 11 (1), 1–8. https://doi.org/10.1038/s41467-020-18531-4.

Ewans, K., Jonathan, P., 2014. Evaluating environmental joint extremes for the offshore industry using the conditional extremes model. J. Mar. Syst. 130, 124–130. https://doi.org/10.1016/j.jmarsys.2013.03.007.

Feng, Y., Shi, P., Qu, S., Mou, S., Chen, C., Dong, F., 2020. Nonstationary flood coincidence risk analysis using time-varying copula functions. Sci. Rep. 10 (1), 1–12. https://doi.org/10.1038/s41598-020-60264-3.

Ghanbari, M., Arabi, M., Kao, S.C., Obeysekera, J., Sweet, W., 2021. Climate change and changes in compound coastal-riverine flooding hazard along the US coasts. Earth's Future 9 (5), e2021EF002055. https://doi.org/10.1029/2021EF002055.

Gori, A., Lin, N., Smith, J., 2020. Assessing compound flooding from landfalling tropical cyclones on the North Carolina coast. Water Resour. Res. 56 (4), e2019WR026788 https://doi.org/10.1029/2019WR026788.

Hallegatte, S., Green, C., Nicholls, R.J., Corfee-Morlot, J., 2013. Future flood losses in major coastal cities. Nat. Clim. Change 3 (9), 802–806. https://doi.org/10.1038/nclimate1979.

Hendry, A., Haigh, I.D., Nicholls, R.J., Winter, H., Neal, R., Wahl, T., Joly-Laugel, A., Darby, S., 2019. Assessing the characteristics and drivers of compound flooding events around the UK coast. Hydrol. Earth Syst. Sci. 23 (7), 3117–3139. https://doi.org/10.5194/hess-23-3117-2019.

Hervouet, J.-M., 2007. Hydrodynamics of Free Surface Flows: Modelling with the Finite Element Method. John Wiley & Sons. https://doi.org/10.1002/9780470319628.

Ikeuchi, H., Hirabayashi, Y., Yamazaki, D., Muis, S., Ward, P.J., Winsemius, H.C., Verlaan, M., Kanae, S., 2017. Compound simulation of fluvial floods and storm surges in a global coupled river-coast flood model: model development and its application to 2007 Cyclone Sidr in Bangladesh. J. Adv. Model. Earth Syst. 9 (4), 1847–1862. https://doi.org/10.1002/2017MS000943.

Inoue, A., Jin, L., Rossi, B., 2017. Rolling window selection for out-of-sample forecasting with time-varying parameters. J. Econom. 196 (1), 55–67. https://doi.org/10.1016/j.jeconom.2016.03.006.

Jalili Pirani, F., Najafi, M.R., 2022. Multivariate analysis of compound flood hazard across Canada's atlantic, pacific and great lakes coastal areas. Earth's Future 10 (8), e2022EF002655. https://doi.org/10.1029/2022EF002655.

Jiang, H., Bai, X., Song, G., Luo, M., Ma, X., 2021. Comparing trivariate models for coastal winds and waves accounting for monthly seasonality. Appl. Ocean Res. 117, 102959 https://doi.org/10.1016/j.apor.2021.102959.

Kontgis, C., Schneider, A., Fox, J., Saksena, S., Spencer, J.H., Castrence, M., 2014. Monitoring peri-urbanization in the greater Ho Chi Minh City metropolitan area. Appl. Geogr. 53, 377–388. https://doi.org/10.1016/j.apgeog.2014.06.029.

Kumbier, K., Carvalho, R.C., Vafeidis, A.T., Woodroffe, C.D., 2018. Investigating compound flooding in an estuary using hydrodynamic modelling: a case study from the Shoalhaven River, Australia. Nat. Hazards Earth Syst. Sci. 18 (2), 463–477. https://doi.org/10.5194/nhess-18-463-2018.

Kundzewicz, Z.W., Robson, A., 2004. Change detection in hydrological records—a review of the methodology/revue méthodologique de la détection de changements dans les chroniques hydrologiques. Hydrol. Sci. J. 49 (1), 7–19. https://doi.org/10.1623/hysj.49.1.7.53993.

Kwon, H.H., Lall, U., 2016. A copula-based nonstationary frequency analysis for the 2012–2015 drought in California. Water Resour. Res. 52 (7), 5662–5675. https://doi.org/10.1002/2016WR018959.

Li, F., Zhou, J., Liu, C., 2018. Statistical modelling of extreme storms using copulas: a comparison study. Coast. Eng. 142, 52–61. https://doi.org/10.1016/j.coastaleng.2018.09.007.

Lucey, J.T., Gallien, T.W., 2022. Characterizing multivariate coastal flooding events in a semi-arid region: the implications of copula choice, sampling, and infrastructure. Nat. Hazards Earth Syst. Sci. 22 (6), 2145–2167. https://doi.org/10.5194/nhess-22-2145-2022.

Manly, B.F., 2018. Randomization, Bootstrap and Monte Carlo Methods in Biology: Texts in Statistical Science. chapman and hall/CRC, New York. https://doi.org/10.1201/9780429329203.

Masina, M., Lamberti, A., Archetti, R., 2015. Coastal flooding: a copula based approach for estimating the joint probability of water levels and waves. Coast. Eng. 97, 37–52. https://doi.org/10.1016/j.coastaleng.2014.12.010.

Metropolis, N., Ulam, S., 1949. The Monte Carlo method. J. Am. Stat. Assoc. 44 (247), 335–341. https://doi.org/10.1080/01621459.1949.10483310.

Murthy, K., 2004. Monte Carlo Methods in Statistical Physics. Universities Press. https://doi.org/10.1007/978-3-642-82803-4.

Myhre, G., Alterskjær, K., Stjern, C.W., Hodnebrog, Ø., Marelle, L., Samset, B.H., Sillmann, J., Schaller, N., Fischer, E., Schulz, M., 2019. Frequency of extreme precipitation increases extensively with event rareness under global warming. Sci. Rep. 9 (1), 1–10. https://doi.org/10.1038/s41598-019-52277-4.

Nguyen, H.Q., Radhakrishnan, M., Bui, T.K.N., Tran, D.D., Ho, L.P., Tong, V.T., Huynh, L. T.P., Chau, N.X.Q., Ngo, T.T.T., Pathirana, A., 2019. Evaluation of retrofitting responses to urban flood risk in Ho Chi Minh City using the motivation and ability (MOTA) framework. Sustain. Cities Soc. 47, 101465 https://doi.org/10.1016/j.scs.2019.101465.

Önöz, B., Bayazit, M., 2012. Block bootstrap for Mann–Kendall trend test of serially dependent data. Hydrol. Process. 26 (23), 3552–3560. https://doi.org/10.1002/hyp.8438.

Pasquier, U., He, Y., Hooton, S., Goulden, M., Hiscock, K.M.J.N.H., 2019. An integrated 1D–2D hydraulic modelling approach to assess the sensitivity of a coastal region to compound flooding hazard under climate change. Nat. Hazards 98 (3), 915–937. https://doi.org/10.1007/s11069-018-3462-1.

Pham, K.N., 2009. Climate change, sea level rise scenarios for Vietnam. In: Hanoi: MONRE. https://www.preventionweb.net/publication/climate-change-sea-level-rise-scenarios-vietnam. (Accessed 20 January 2023).

Rasmussen, C.E., Ghahramani, Z., 2003. Bayesian Monte Carlo. Adv. Neural Inf. Process. Syst. 505–512. In: https://proceedings.neurips.cc/paper/2002/file/24917db15c4e37e421866448c9ab23d8-Paper.pdf.

Sadegh, M., Moftakhari, H., Gupta, H.V., Ragno, E., Mazdiyasni, O., Sanders, B., Matthew, R., AghaKouchak, A., 2018. Multihazard scenarios for analysis of compound extreme events. Geophys. Res. Lett. 45 (11), 5470–5480. https://doi.org/10.1029/2018GL077317.

Sadegh, M., Ragno, E., AghaKouchak, A., 2017. Multivariate Copula Analysis Toolbox (MvCAT): describing dependence and underlying uncertainty using a Bayesian framework. Water Resour. Res. 53 (6), 5166–5183. https://doi.org/10.1002/2016WR020242.

Salvadori, G., Tomasicchio, G., D'Alessandro, F., 2014. Practical guidelines for multivariate analysis and design in coastal and off-shore engineering. Coast. Eng. 88, 1–14. https://doi.org/10.1016/j.coastaleng.2014.01.011.

Sarhadi, A., Ausín, M.C., Wiper, M.P., Touma, D., Diffenbaugh, N.S., 2018. Multidimensional risk in a nonstationary climate: joint probability of increasingly severe warm and dry conditions. Sci. Adv. 4 (11), eaau3487 https://doi.org/10.1126/sciadv.aau3487.

Scussolini, P., Tran, T.V.T., Koks, E., Diaz-Loaiza, A., Ho, P.L., Lasage, R., 2017. Adaptation to sea level rise: a multidisciplinary analysis for Ho Chi Minh City. Vietnam. Water Resour. Res. 53 (12), 10841–10857. https://doi.org/10.1002/2017WR021344.

Shi, S., Yang, B., Jiang, W., 2022. Numerical simulations of compound flooding caused by storm surge and heavy rain with the presence of urban drainage system, coastal dam and tide gates: a case study of Xiangshan. China. Coast. Eng. 172, 104064 https://doi.org/10.1016/j.coastaleng.2021.104064.

Sklar, A., 1959. Fonctions de Répartition à n Dimensions et Leurs Marges, vol. 8. Publications de l'Institut Statistique de l'Université de Paris, pp. 229–231.

Tangang, F., Juneng, L., Cruz, F., Chung, J.X., Ngai, S.T., Salimun, E., Mohd, M.S.F., Santisirisomboon, J., Singhruck, P., PhanVan, T., 2020. Multi-model projections of precipitation extremes in Southeast Asia based on CORDEX-Southeast Asia simulations. Environ. Res. 184, 109350 https://doi.org/10.1016/j.envres.2020.109350.

Tanim, A.H., Goharian, E., 2021. Developing a hybrid modeling and multivariate analysis framework for storm surge and runoff interactions in urban coastal flooding. J. Hydrol. 595, 125670 https://doi.org/10.1016/j.jhydrol.2020.125670.

Tiggeloven, T., De Moel, H., Winsemius, H.C., Eilander, D., Erkens, G., Gebremedhin, E., Diaz Loaiza, A., Kuzma, S., Luo, T., Iceland, C., 2020. Global-scale benefit–cost analysis of coastal flood adaptation to different flood risk drivers using structural measures. Nat. Hazards Earth Syst. Sci. 20 (4), 1025–1044. https://doi.org/10.5194/nhess-20-1025-2020.

Trinh-Tuan, L., Matsumoto, J., Tangang, F.T., Juneng, L., Cruz, F., Narisma, G., Santisirisomboon, J., Phan-Van, T., Gunawan, D., Aldrian, E., 2019. Application of quantile mapping bias correction for mid-future precipitation projections over Vietnam. Inside Solaris. https://doi.org/10.2151/sola.2019-001.

Utsumi, N., Kim, H., 2022. Observed influence of anthropogenic climate change on tropical cyclone heavy rainfall. Nat. Clim. Change 12 (5), 436–440. https://doi.org/10.1038/s41558-022-01344-2.

Vachaud, G., Quertamp, F., Phan, T.S.H., Ngoc, T.D.T., Nguyen, T., Luu, X.L., Nguyen, A. T., Gratiot, N., 2019. Flood-related risks in Ho Chi Minh city and ways of mitigation. J. Hydrol. 573, 1021–1027. https://doi.org/10.1016/j.jhydrol.2018.02.044.

van den Hurk, B., van Meijgaard, E., de Valk, P., van Heeringen, K.-J., Gooijer, J., 2015. Analysis of a compounding surge and precipitation event in The Netherlands. Environ. Res. Lett. 10 (3), 035001 https://doi.org/10.1088/1748-9326/10/3/035001.

Wahl, T., Jain, S., Bender, J., Meyers, S.D., Luther, M.E., 2015. Increasing risk of compound flooding from storm surge and rainfall for major US cities. Nat. Clim. Change 5 (12), 1093–1097. https://doi.org/10.1038/nclimate2736.

Wahl, T., Mudersbach, C., Jensen, J., 2012. Assessing the hydrodynamic boundary conditions for risk analyses in coastal areas: a multivariate statistical approach based on Copula functions. Nat. Hazards Earth Syst. Sci. 12 (2), 495–510. https://doi.org/10.5194/nhess-12-495-2012.

Zar, J.H., 2005. Spearman rank correlation. Encyclopedia of biostatistics 7. https://doi.org/10.1002/0470011815.b2a15150.

Zhang, Y., Kim, C.-W., Beer, M., Dai, H., Soares, C.G., 2018. Modeling multivariate ocean data using asymmetric copulas. Coast. Eng. 135, 91–111. https://doi.org/10.1016/j.coastaleng.2018.01.008.

Zhang, Y.J., Ye, F., Yu, H., Sun, W., Moghimi, S., Myers, E., Nunez, K., Zhang, R., Wang, H., Roland, A., 2020. Simulating compound flooding events in a hurricane. Ocean Dynam. 70 (5), 621–640. https://doi.org/10.1007/s10236-020-01351-x.

Zscheischler, J., Westra, S., Van Den Hurk, B.J., Seneviratne, S.I., Ward, P.J., Pitman, A., AghaKouchak, A., Bresch, D.N., Leonard, M., Wahl, T., 2018. Future climate risk from compound events. Nat. Clim. Change 8 (6), 469–477. https://doi.org/10.1038/s41558-018-0156-3.